analytical chemistry

Article

Cite This: Anal. Chem. 2019, 91, 6769−6774

pubs.acs.org/ac

Nanoparticles-Enabled Surface-Enhanced Imaging Ellipsometry for Amplified Biosensing

Zhilong Wang,[†,⊥] Yunlei Xianyu,[§,⊥] Wei Liu,[‡,⊥] Yike Li,[‡] Zhaoxia Cai,[†] Xing Fu,[†] Gang Jin,[‡] Yu Niu,[*,‡] Cai Qi,[*,∥] and Yiping Chen[*,†]

[†]College of Food Science and Technology, Huazhong Agricultural University, Wuhan, 430070, China

[‡]NML, Beijing Key Laboratory of Engineered Construction and Mechanobiology, Institute of Mechanics, Chinese Academy of Sciences, Beijing 100190, China

[§]National Center for Nanoscience and Technology, Beijing 100190, China

[∥]Guizhou Jinjiu Biotech. Co. Ltd., Guiyang 550005, China

Supporting Information

ABSTRACT: The main issues of imaging ellipsometry-based biosensing for small molecules are the low sensitivity and narrow detection range due to the low molecular weight of small molecules that results in a negligible signal. To meet this challenge, we theoretically investigated the deciding factors of the ellipsometry signal and further applied the theory to guide the design of ellipsometry-based biosensor using metal nanoparticles that have a high dielectric constant. Significant signal amplification effects can be achieved by using nanoparticle labels including magnetic nanoparticles and gold nanoparticles. Guided by the theory, we have developed a sensitive surface-enhanced imaging ellipsometry (SEIE)-biosensor for detecting chloramphenicol in real milk sample with high sensitivity (with a limit of detection of 6 pg/mL) and broaden detection range. This nanoparticles-enabled SEIE not only greatly improves the sensitivity of conventional imaging ellipsometry-based biosensors but also retains the advantages of conventional methods in terms of automated and convenient operation, providing an effective strategy for detection of trace small molecules in complex samples that holds great promise in scientific research, clinical diagnosis, and food safety.

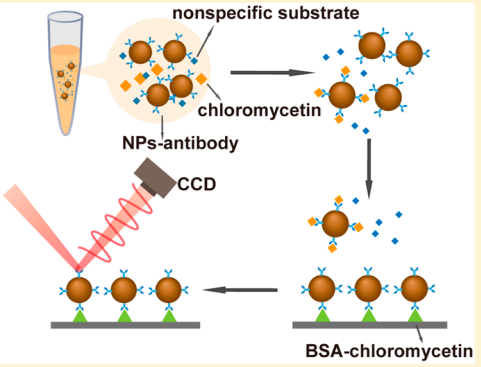

Ellipsometry as an optically noninvasive method has attracted researchers' interests for biosensing due to its advantages such as high spatial resolution, fast data acquisition, and simple operation.[1−5] Ellipsometry is a powerful tool for measuring the thickness of a film with high resolution (about 1 nm), demonstrating it as a label-free strategy for biosensing.[6,7] Theoretically, the ellipsometry signal relates to three factors including the thickness, the dielectric constant, and the surface coverage ratio of film/substance.[3,8] We have developed a microfluidic imaging ellipsometry biosensor that has the merits of both microfluidic technology and imaging ellipsometry including low sample consumption, automated operation, multiplexed, and label-free detection.[9] However, it is still incapable of detecting trace targets because of the limited sensitivity and detection range of conventional ellipsometry, where the elipsometry signal comes from biomolecules (protein or DNA) whose molecular weights are relatively low that contribute little to the ellipsometry signal.[10,11] To improve the sensitivity of ellipsometry, many signal amplification strategies have been developed. For example, our group has developed the secondary antibody-mediated sandwich strategy to increase the thickness of the substance to amplify the ellipsometry signal.[12] Despite that, the detection of low molecular weight protein biomarkers in serum samples has been achieved, and the signal amplification effect is limited because the size/thickness of antibody is generally less than 20 nm. That confines its ability to amplify the ellipsometry signal for the detection of small molecules that requires a very high sensitivity. It is thus of great need to develop a technique that can boost the sensitivity of conventional ellipsometry biosensors to broaden their applications in detections of both biomacromolecules and small molecules with a high sensitivity and broad detection range.

With the burgeoning progress in nanotechnology, nanoparticles (NPs) have been widely used in biosensors as signal readouts or signal amplifiers that greatly improved the analytical performances (sensitivity, speediness, and operation) due to their excellent optical, magnetic, catalytic, or electrical properties.[13−16] For example, gold nanoparticles (AuNPs) and magnetic nanoparticles (MNPs) have been widely used for point-of-care testing due to the plasmon resonance properties of AuNPs[17−20] and the magnetic separation and anti-

Received: February 15, 2019
Accepted: May 3, 2019
Published: May 3, 2019

DOI: 10.1021/acs.analchem.9b00846
Anal. Chem. 2019, 91, 6769−6774

interference ability of MNPs.[21−26] Guided by the principle that the thickness and dielectric constant of the film/substance dictate the signals of ellipsometry, we introduce NPs that are beneficial for the enhancement of the ellipsometry signal. With two distinct advantages, NPs are expected to greatly amplify the ellipsometry signal. First, the size and mass of NPs are much larger than that of proteins (antibody or antigen), which can greatly enhance the thickness resolution of elliptic polarized light contributing to amplify the ellipsometry signal. Second, NPs can have unique optical features that can directly change the elliptic polarized light or have synergistic effects to enhance the ellipsometry signal, which may also contribute to enhancing the ellipsometry signal.[15,27−30]

In this study, we theoretically investigated the effect of NPs on the ellipsometry signal and revealed the principle of NPs-based imaging ellipsometry for amplified biosensing (Scheme 1A). The theoretical study shows that both the diameter and the dielectric constant of NPs play significant roles in the output of the ellipsometry signal. Based on the proposed principle, we developed a surface-enhanced imaging ellipsometry (SEIE) by using MNPs and AuNPs for the ultrasensitive detection of chloramphenicol in milk samples (Scheme 1B−C). In this strategy, AuNPs and MNPs have significant thickness and specific surface area that contribute to the amplified ellipsometry signal for the small molecule detection. Besides, the higher dielectric constant (εNPs) of MNPs or AuNPs compared with that of air is also beneficial for the enhancement of the ellipsometry signal.[31−33] In addition, this SEIE-biosensor is based on a sandwich mode rather than the one-step immuno-reaction in conventional method that can circumvent the nonspecific issue. To the best of our knowledge, it is the first report that theoretically investigates the interplay between NPs and ellipsometry signal which further guides the design of NPs-based biosensors to improve the sensitivity and broaden the detection range of the conventional imaging ellipsometry.

Scheme 1. Nanoparticles-Enabled Surface-Enhanced Imaging Ellipsometry for Amplified Biosensing[a]

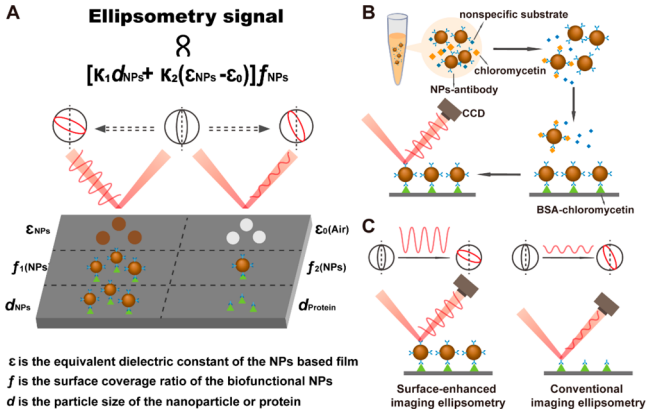

[a](A) Parameters of NPs that decide the ellipsometry signal including the dielectric constant, the surface coverage ratio, and the particle size; (B) Schematic illustration of the SEIE-biosensor for detection of chloramphenicol; (C) Comparison between surface-enhanced imaging ellipsometry and conventional imaging ellipsometry for detection of chloramphenicol.

EXPERIMENTAL SECTION

Preparation of MNP_{30}-Ab_1 Conjugate. The process of the preparation of MNP_{30}-Ab_1 conjugate was based on our previous work with some modifications.[23] 0.5 mg of MNP_{30} was added into 50 μL of activated buffer (80 nM MES, pH 6.0), and then 5 μL of EDC (10 mg mL^{-1}) and 5 μL of NHS (10 mg mL^{-1}) were added into the MNP_{30} solution. After the above mixture solution was activated for about 30 min, 1000 μL of coupling buffer PBS (pH 7.4, 0.01M) was added into the activated MNP_{30} solution. 0.02 mg of Ab_1 was added into the activated MNP_{30}, and the mixture solution was gently stirred for 2 h at room temperature, followed by the addition of 100 μL of 3% BSA for 0.5 h. We collected the MNP_{30}-Ab_1 conjugate from the free Ab_1 by magnetic separation using the SuperMag separator at 4 °C for 24 h, and resuspend it using 500 μL of PBST. The magnetic separation step was repeated for three times. Finally, MNP_{30}-Ab_1 conjugate was resuspended using 500 μL of PBS solution (pH 7.4, 0.01M, 0.01% BSA) and was stored at 4 °C for further use.

Preparation of Au-Ab_1 Conjugate. The method for synthesis of 30 nm Au NPs and preparation of Au-Ab_1 conjugate were based on the previous work in our group.[34]

The Procedure of IE-Biosensor for Detection of Chloramphenicol. The preparation of carboxyl group-modified silicon wafers was referred to our previous works.[35,36] BSA-chloramphenicol conjugate (0.5 mg/mL) was covalently immobilized on the modified silicon substrate by EDC/NHS-mediated condensation reaction at 1 μL min^{-1} for 10 min, followed by washing with PBST. Then, the blocking buffer (PBS solution with 3% BSA) was injected at 1 μL min^{-1} for 30 min to block the nonspecific binding sites. After that, 50 μL of chloramphenicol solution or samples was mixed with 50 μL of Ab_1 (0.05 mg/mL) for 15 min, and this mixture solution was injected into flow channels at 2 μL min^{-1} for 10 min and rinsed with PBST for 2 min. After that, the grayscale images of the fabricated protein microarray and thickness distribution of the protein layers were captured by the imaging ellipsometer.

The Procedure of SEIE-Biosensor for Detection of Chloramphenicol. The immobilization of BSA-chloramphenicol conjugate on silicon wafers and the blocking step were the same as that of the IE biosensor. After that, 50 μL of the sample was added into 50 μL of MNP_{30}-Ab_1 (0.1 mg/mL), and the mixture solution was shaken at room temperature for 15 min. This mixture solution was then injected into flow channels at 2 μL min^{-1} for 10 min and rinsed with PBST for 2 min. After that, the grayscale images of the fabricated nanoparticles microarray and thickness distribution of the nanoparticle layers were captured by the imaging ellipsometer.

Analytical Performance of IE-Biosensor and SEIE-Biosensor for Detection of Chloramphenicol. We added 50 μL of different concentrations of chloramphenicol (0, 0.01, 0.1, 1, 10, and 100 ng/mL) into 50 μL of MNP_{30}-Ab_1 (0.1 mg/mL) for the sensitivity test. The sensitivity test included the calibration curve and limit of detection (LOD). The calibration curve was performed under the optimized condition to detect the standard samples of chloramphenicol from 0.01 to 100 ng mL^{-1}, and each concentration was analyzed at least three times. We calculated the LOD based on the calibration curve with $3S/M$, where S is the value of the standard deviation of blank samples; M is the slope of standard curve within a low concentration range. In the selectivity test, thiamphenicol,

DOI: 10.1021/acs.analchem.9b00846
Anal. Chem. 2019, 91, 6769−6774

cephalosporin, tetracycline, sulfadimidine, and gentamicin were employed as analogues to investigate the specificity of SEIE-biosensor for detection of chloramphenicol. The concentration of these analogues is 500 ng/mL, and the concentration of chloramphenicol is 50 ng/mL. A series of different concentrations of chloramphenicol (0.1, 0.5, 1, 10, 50, and 100 ng/mL) were added into the blank milk samples for the recovery study.

Milk Samples analysis. Twenty blind samples were obtained from Chinese Academy of Inspection and Quarantine. The concentrations of chloramphenicol in these samples were previously detected by HPLC−MS according to the PRC National Standard (GB 29688−2013). These blind samples were diluted two fold by PBS, and they were analyzed by the IE-biosensor and SEIE-biosensor, respectively. Each sample was assayed three times (n = 3).

RESULTS AND DISCUSSION

Theoretical Study of the Interplay between NPs and the Ellipsometry Signal. When NPs adsorb on the film, both the size of the NPs(d_{NPs}) and the dielectric constants (ε_{NPs}) come into play. The dielectric constant of the equivalent NPs-based film can be approximated by Maxwell Garnett mixing formula[37]

$$\varepsilon = \varepsilon_0 \frac{1 + 2f\frac{\varepsilon_{Np} - \varepsilon_0}{\varepsilon_{NP} + 2\varepsilon_0}}{1 - f\frac{\varepsilon_{Np} - \varepsilon_0}{\varepsilon_{NP} + 2\varepsilon_0}} \quad (1)$$

and the equivalent thickness can be approximated by

$$d = fd_{NPs} \quad (2)$$

Where ε is the equivalent dielectric constant of the NPs-based film, d is the equivalent thickness, f is the surface coverage ratio of the NPs which satisfies $0 \le f \le 1$, and ε_0 is the dielectric constant of the medium. Since the imaging ellipsometry-based biosensor works under the external reflection condition, the medium is air in this study which gives $\varepsilon 0 \approx 1$.

The ellipsometric parameter variation $\delta\rho/\rho$ from the equivalent film can be given by (see the Supporting Information (SI))

$$\frac{\delta\rho}{\rho} = \kappa_1\delta d + \kappa_2\delta\varepsilon \quad (3)$$

where k_1 and k_2 are the complex constants determined by the substrate without NPs.

According to eq 1), the variation of the equivalent dielectric constant $\delta\varepsilon$ on the bare substrate (where f = 0) caused by NPs adsorption can be approximated by

$$\delta\varepsilon = 3\frac{\varepsilon_{Np} - \varepsilon_0}{\varepsilon_{NP} + 2\varepsilon_0}\delta f \quad (4)$$

Taking eqs 2 and 4 into eq 3), we have

$$\frac{\delta\rho}{\rho} = \left[\kappa_1 d_{NPs} + 3\kappa_2\frac{\varepsilon_{Np} - \varepsilon_0}{\varepsilon_{NP} + 2\varepsilon_0}\right]\delta f \quad (5)$$

Or in terms of Ψ and Δlanguage, we have

$$\delta\psi = \left(\frac{1}{2}\sin 2\psi\right)\mathrm{Re}\left(\frac{\delta\rho}{\rho}\right) = \left(\frac{1}{2}\sin 2\psi\right)\mathrm{Re}\left[\kappa_1 d_{NPs} + 3\kappa_2\frac{\varepsilon_{Np} - \varepsilon_0}{\varepsilon_{NP} + 2\varepsilon_0}\right]\delta f$$

$$\delta\Delta = \mathrm{Im}\left(\frac{\delta\rho}{\rho}\right) = \mathrm{Im}\left[\kappa_1 d_{NPs} + 3\kappa_2\frac{\varepsilon_{Np} - \varepsilon_0}{\varepsilon_{NP} + 2\varepsilon_0}\right]\delta f \quad (6)$$

On the one hand, eq 6) suggests that when NPs are introduced at the sensing surface, the signal is determined by the surface coverage ratio of NPs and its variation is proportional to the change in the surface coverage ratio. On the other hand, as is indicated in eqs 5) and 6, for a given surface coverage ratio, the amplification effect is determined by the size of NPs and the $\left(\frac{\varepsilon_{Np} - \varepsilon_0}{\varepsilon_{NP} + 2\varepsilon_0}\right)$, which implies that the dielectric constant difference between NPs and the air is important for the signal amplification.

Based on the theoretical study, we introduce MNPs and AuNPs into the sensing surface of the ellipsometry-biosensors to enhance the ellipsometry signals for detecting small molecules because metal NPs have large size and dielectric constants due to their high extinction coefficients.

Characterizations of MNPs and AuNPs on Silicon Substrate. We first employed scanning electron microscope (SEM) to characterize the adsorbed MNPs on silicon substrate. The amount of MNP_{30} on silicon substrate relates to the concentration of MNP_{30}-goat antirabbit IgG conjugate. SEM images show that MNP_{30} can absorb on silicon substrate through the antigen−antibody interaction (Figure 1A). When the concentration of MNP_{30}-goat antirabbit IgG conjugate decreased, the amount of MNP_{30}-goat antirabbit IgG conjugate adsorbed on silicon substrate also reduced (Figure 1B−C). We also observed the surface of silicon substrate in microfluidic channel using SEM (Figure 1D−F), and the brightness related to the concentration of MNPs-goat anti rabbit IgG conjugate

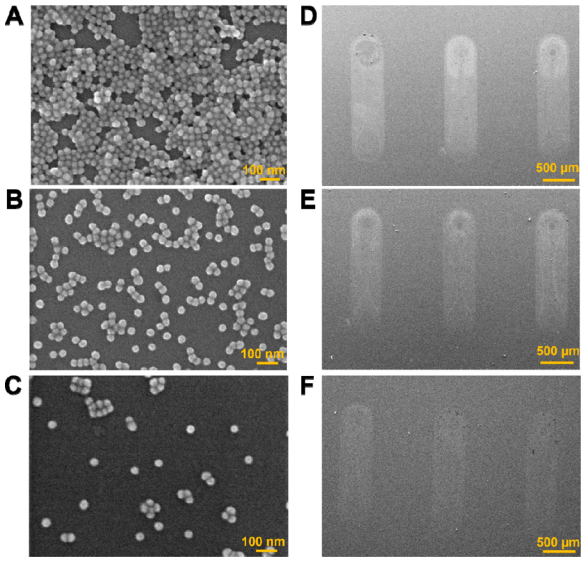

Figure 1. SEM characterizations of MNPs coated on silicon substrate. The scale bars are 100 nm in panels (A)−(C), and 500 μm in panels (D)−(F). Rabbit anti human IgG (50 μg/mL) was coated on the surface of silicon substrate. The concentration of MNPs-goat antirabbit IgG conjugate was 0.5 mg/mL in panels (A) and (D), 0.1 mg/mL in panels (B) and (E), and 0.05 mg/mL in panels (C) and (F).

DOI: 10.1021/acs.analchem.9b00846
Anal. Chem. 2019, 91, 6769−6774

adsorbed on the surface of silicon substrate. The images showed that as the concentration of MNPs-IgG increased, it presented a much stronger brightness of the microfluidic channel, suggesting that the introduction of MNPs is an effective way to enhance the ellipsometry signal.

We used MNPs and AuNPs to investigate their signal amplification effects. Compared with MNPs of 30 nm, less MNPs of 150 nm were captured on the silicon substrate by antigen−antibody interaction under the same reaction condition (SI Figure S1A). The poor capture efficiency of large MNPs may be that they have a higher fluid shear stress than the small MNPs, considering that the fluid shear stress of NPs depends on their size. When the size of MNPs is 150 nm, the fluid shear stress can outcompete the antigen−antibody interaction that results in the poor absorption on silicon substrate. Consistent with the MNP_{30}, we found that AuNPs of 30 nm can be captured on silicon substrate (SI Figure S1B), and the ellipsometry signal can be significantly enhanced for detection of rabbit antihuman IgG (SI Figure S2). We thus employed MNP_{30} and $AuNP_{30}$ for the signal amplification of the ellipsometry signal in this biosensor.

Apart from SEM characterizations, we also employed atomic force microscopy (AFM) to characterize the MNP_{30} on silicon substrate. We found that the MNP_{30}-goat antirabbit IgG conjugate or goat antirabbit IgG can absorb on silicon substrate coated with rabbit antihuman IgG by the specific antibody−antigen recognition. The adsorption capacity also related to the concentration of MNP_{30}-goat antirabbit IgG conjugate used in this immune reaction (Figure 2A−B). The AFM images shows that the overall size of MNP_{30}-goat antirabbit IgG conjugate was about 50 nm, and the size of goat antirabbit IgG was about 5 nm (Figure 2C), demonstrating the

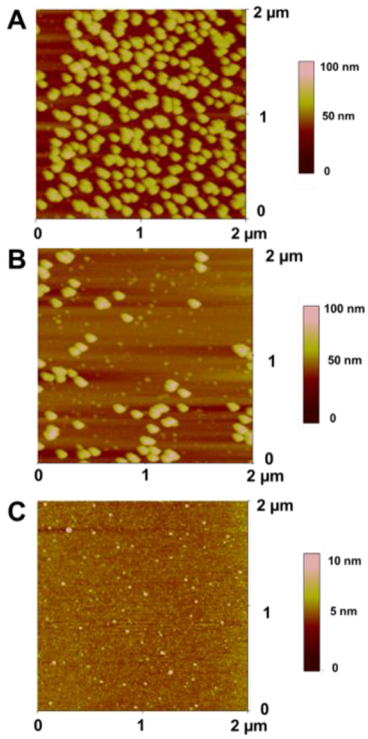

Figure 2. AFM characterizations of MNPs coated on silicon substrate. The silicon substrate was coated by 50 μg/mL of rabbit anti human IgG. The concentration of MNPs-goat antirabbit IgG conjugate was (A) 0.5 mg/mL; (B) 0.1 mg/mL; and (C) 0.5 mg/mL.

effectiveness of the adsorption of NPs and the antibody−antigen interaction.

Comparison between SEIE and Conventional IE for Chloramphenicol Detection. In the SEIE-biosensor, the concentration of chloramphenicol determines the amount of MNPs or AuNPs attached on silicon substrate, resulting in the change of ellipsometry image signal. Similarly, the ellipsometry image signal in conventional IE is dictated by the amount of Ab absorbed on the substrate (Scheme 1C). The ellipsometry image signal decreased in SEIE when the concentration of chloramphenicol changed from 0.01 ng/mL to 100 ng/mL (Figure 3A and D) because a competitive immunoassay was

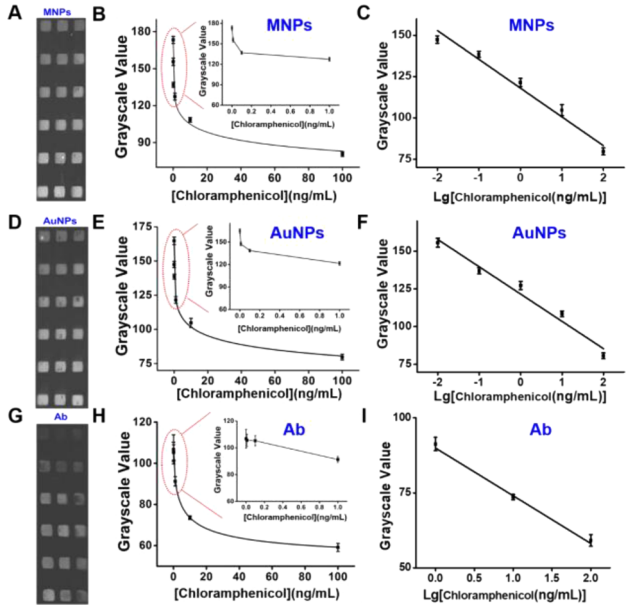

Figure 3. Sensitivity of the SEIE-biosensor and conventional IE-biosensor for chloramphenicol detection. (A) The grayscale image in MNPs-implemented SEIE; (B)−(C) The calibration curve and the linear range of MNPs-implemented SEIE-biosensor for quantitative chloramphenicol detection; (D) The grayscale image in AuNPs-implemented SEIE; (E)−(F) The calibration curve and the linear range of AuNPs-implemented SEIE for quantitative chloramphenicol detection; (G) The grayscale image in conventional IE; (H)−(I) The calibration curve and the linear range for quantitative chloramphenicol detection in conventional IE.

used in the SEIE-biosensor for detection of chloramphenicol. The ellipsometry image signal was inversely proportional to the concentration of chloramphenicol. In conventional IE-biosensor, the ellipsometry image signal decreased when the concentration of chloramphenicol changed from 0.1 to 100 ng/mL, showing a lower sensitivity compared with SEIE (Figure 3G).

To achieve quantitative detection, we employed the grayscale value to quantify the change of the ellipsometry image signal. The gray scale value decreased when the concentration of chloramphenicol increased from 0.01 to 100 ng/mL in SEIE (Figure 3A and D). The limit of detection (LOD = $3S/M$, where S is the value of the standard deviation of blank samples; M is the slope of standard curve within a low concentration range) for detection of chloramphenicol is 0.006 ng/mL(LOD = $3S/M$, S = 2.8, M = 1300) in MNPs-implemented SEIE-biosensor (Figure 3B), and the linear range is 0.01 ng/mL to 100 ng/mL with a linear equation of Y =

DOI: 10.1021/acs.analchem.9b00846
Anal. Chem. 2019, 91, 6769−6774

−17.4X+118.1 (X = lg[chloramphenicol (ng/mL)], R^2 = 0.96) (Figure 3C). The LOD of AuNPs-implemented SEIE biosensor for detection of chloramphenicol is 0.005 ng/mL(LOD = 3S/M, S = 3.01, M = 1730) (Figure 3E), and the linear range is 0.01 ng/mL to 100 ng/mL (Figure 3E) with the linear equation of Y = −18.1X + 121.6 (X = lg-[chloramphenicol (ng/mL)], R^2 = 0.96) (Figure 3F). We compared the analytical performances of NPs-implemented SEIE with traditional IE. The LOD of conventional IE for detection of chloramphenicol is 0.43 ng/mL (LOD = 3S/M, S = 2.2, M = 15.5), and the linear range is from 1 ng/mL to 100 ng/mL (Figure 3H) with the linear equation of Y = −15.9X + 89.9 (X = lg[chloramphenicol (ng/mL)], R^2 = 0.98) (Figure 3I). The sensitivity and the linear range of NPs-implemented SEIE have been improved by 2 orders of magnitude compared with conventional IE. Considering that chloramphenicol is a prohibited antibiotic in agriculture and the maximum residue limit in food products should be under 0.01 ng/mL, conventional IE is hardly to achieve such a high sensitivity for detection of chloramphenicol in food products.[38,39] In contrast, NPs-implemented IE can greatly amplify the signal of conventional IE biosensor to meet the requirement for the detection of chloramphenicol. Two key factors contribute to the high sensitivity of SEIE-biosensor. One is the high dielectric constants of MNPs/AuNPs that can achieve amplified ellipsometry signals. The other is the larger size of MNPs/AuNPs over antibodies in conventional IE that can dramatically improve the ellipsometry signal.

We also investigated the selectivity, accuracy, repeatability, and stability of this SEIE-biosensor. We employed other antibiotics as analogues to evaluate its anti-interference. The grayscale value from chloramphenicol is much lower than that from other analogues (SI Figure S3). Interestingly, we found that grayscale value from the thiamphenicol is lower than that of three other analogues because the molecular structure of thiamphenicol is similar to that of chloramphenicol. It suggested that this NPs-mediated signal amplification does not affect the specificity of the immuno-recognition between antibody and antigen, showing good specificity for detection of chloramphenicol.

To further study the accuracy and repeatability, we employed this sensor for detection of a series of spiked milk samples (SI Table S1). The recovery rates under different spiked concentrations of chloramphenicol were from 92.3% to 130%, suggesting that the SEIE-biosensor has a good accuracy. The intraindividual coefficient of variation (intra-CV) was under 10.4%, and the inter-CV within 2 weeks was both below 13.2%, showing that this SEIE-biosensor has a good stability and repeatability for detection of chloramphenicol (SI Table S1).

Milk Sample Analysis. We employed this SEIE and conventional IE to detect chloramphenicol in 20 real milk samples to demonstrate the practical application of this SEIE. The concentration of chloramphenicol in these real milk samples were predetermined by high performance liquid chromatography−mass spectrum (HPLC−MS), a gold standard method for detection of trace antibiotics in food samples. Sample 1, samples 4−9, sample 12, samples 15−17, and sample 19 were detected to be chloramphenicol-positive by both HPLC−MS and SEIE, and other samples are detected to be chloramphenicol-negative (Figure 4A). In contrast, only sample 1, samples 7−8, and samples 15−17 were detected to be chloramphenicol-positive by IE-biosensor (Figure 4A), and

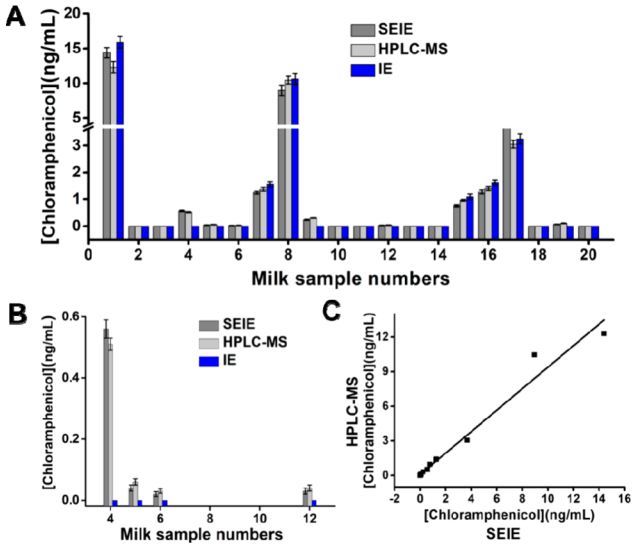

Figure 4. SEIE, HPLC−MS and conventional IE for detection of chloramphenicol in real milk samples. (A) and (B) Quantitative detection of chloramphenicol in real milk samples using SEIE, HPLC−MS, and IE-biosensor; (C) The comparison of chloramphenicol levels measured by the SEIE and HPLC−MS. The milk samples were from Chinese Academy of Inspection and Quarantine (Beijing, China), and the concentration of chloramphenicol in these samples were determined by HPLC−MS.

samples 4−6 and sample 12 were detected to negative by conventional IE, suggesting that the SEIE can improve the false negative issue of conventional IE (Figure 4B). More importantly, the quantitative results of this SEIE for detection of chloramphenicol agree well with those of HPLC−MS (Figure 4C and SI Table S2). Although HPLC−MS is a widely used, highly sensitive, and accurate assay for detection of antibiotic residues in food safety and environmental monitoring, it needs complex sample pretreatment and it is high cost, which limit its further application for large samples screening and on-site detection. In contrast, the SEIE is a straightforward and rapid method that not only retains the merits of conventional IE (automation and high throughput) but also greatly improves the sensitivity, which has great potential in detection of trace hazardous substance in food safety.

CONCLUSION

In conclusion, we have theoretically investigated the principle of NPs-mediated signal amplification for the ellipsometry signal, and further developed a SEIE-biosensor based on MNPs and AuNPs for the ultrasensitive detection of antibiotic residue. This SEIE-biosensor not only improves the analytical performance of conventional imaging ellipsometry-based biosensor, but it also retains many advantages such as convenient and automatic operation. Further work should focus on developing SEIE-mediated molecular diagnostic biosensors for detection of cells, pathogens, and viruses. The SEIE-biosensors developed in this study broaden the application of NPs-based biosensors, and they can become useful tools for the detection of trace analytes in clinical diagnosis, food safety, and environmental monitoring.

DOI: 10.1021/acs.analchem.9b00846
Anal. Chem. 2019, 91, 6769−6774

■ ASSOCIATED CONTENT

Supporting Information

The Supporting Information is available free of charge on the ACS Publications website at DOI: 10.1021/acs.analchem.9b00846.

Materials and apparatus, and additional results including recovery rate and stability of the MNPs-SEIE for detection of chloramphenicol (Table S1), quantitative determinations of chloramphenicol in real milk samples by MNPs-SEIE, convention IE and HPLC−MS (Table S2), the SEM of 150 nm MNPs and 30 nm AuNPs on silicon wafers (Figure S1), MNPs/Au-implemented SEIE-biosensor and conventional IE-biosensor for detection of rabbit antihuman IgG (Figure S2), and the selectivity of MNPs-implemented SEIE-biosensor for detection of chloramphenicol (Figure S3) (PDF)

■ AUTHOR INFORMATION

Corresponding Authors

*(Y.N.) E. mail: niuyu@imech.ac.cn.
*(C.Q.) E. mail: qicaisucceed1@163.com.
*(Y.C.) E. mail: chenyiping@mail.hzau.edu.cn.

ORCID

Xing Fu: 0000-0002-5390-1748
Yu Niu: 0000-0003-2380-1006
Yiping Chen: 0000-0001-9309-2730

Author Contributions

⊥Z.W., Y.X., and W.L. contributed equally this work equally

Notes

The authors declare no competing financial interest.

■ ACKNOWLEDGMENTS

We thank the National Science Foundation of China (81671784) and the Beijing Nova Program (Z181100006218017) for financial support.

■ REFERENCES

(1) Wang, Z. H.; Jin, G. *Anal. Chem.* **2003**, *75*, 6119−6123.
(2) Khansili, N.; Rattu, G.; Krishna, P. M. *Sens. Actuators, B* **2018**, *265*, 35−49.
(3) Jin, G.; Meng, Y. H.; Liu, L.; Niu, Y.; Chen, S.; Cai, Q.; Jiang, T. J. *Thin Solid Films* **2011**, *519*, 2750−2757.
(4) Lisak, G.; Arnebrant, T.; Lewenstam, A.; Bobacka, J.; Ruzgas, T. *Anal. Chem.* **2016**, *88*, 3009−3014.
(5) Garcia-Marin, A.; Abad, J. M.; Ruiz, E.; Lorenzo, E.; Piqueras, J.; Pau, J. L. *Anal. Chem.* **2014**, *86*, 4969−4976.
(6) Shoji, E.; Komiya, A.; Okajima, J.; Kubo, M.; Tsukada, T. *Opt. Laser. Eng.* **2019**, *112*, 145−150.
(7) Niu, Y.; Jin, G. *Protein Cell* **2011**, *2*, 445−455.
(8) Elwing, H. *Biomaterials* **1998**, *19*, 397−406.
(9) Wang, Z. H.; Meng, Y. H.; Ying, P. Q.; Qi, C.; Jin, G. *Electrophoresis* **2006**, *27*, 4078−4085.
(10) Niu, Y.; Jin, G. *Appl. Surf. Sci.* **2013**, *281*, 84−88.
(11) Çağlayan, M. O.; Sayar, F.; Demirel, G.; Garipcan, B.; Otman, B.; ÇElen, B.; Pişkin, E. *Nanomedicine* **2009**, *5*, 152−161.
(12) Li, Y. K.; Liu, W.; Jin, G.; Niu, Y.; Chen, Y. P.; Xie, M. X. *Anal. Chem.* **2018**, *90*, 8002−8010.
(13) Joo, J.; Kwon, D.; Yim, C.; Jeon, S. *ACS Nano* **2012**, *6*, 4375−4381.
(14) Gandhi, S.; Arami, H.; Krishnan, K. M. *Nano Lett.* **2016**, *16*, 3668−3674.
(15) Loynachan, C. N.; Thomas, M. R.; Gray, E. R.; Richards, D. A.; Kim, J.; Miller, B. S.; Brookes, J. C.; Agarwal, S.; Chudasama, V.; McKendry, R. A.; Stevens, M. M. *ACS Nano* **2018**, *12*, 279−288.
(16) Kim, J. H.; Park, J. E.; Lin, M.; Kim, S.; Kim, G. H.; Park, S.; Ko, G.; Nam, J. M. *Adv. Mater.* **2017**, *29*, 1702945.
(17) Aldewachi, H.; Chalati, T.; Woodroofe, M. N.; Bricklebank, N.; Sharrack, B.; Gardiner, P. *Nanoscale* **2018**, *10*, 18−33.
(18) Chiu, N. F.; Chen, C. C.; Yang, C. D.; Kao, Y. S.; Wu, W. R. *Nanoscale Res. Lett.* **2018**, *13*, 152.
(19) Zhou, Y. F.; Ding, L.; Wu, Y. H.; Huang, X. L.; Lai, W. H.; Xiong, Y. H. *TrAC, Trends Anal. Chem.* **2019**, *112*, 147−160.
(20) Chen, X. R.; Liang, Y.; Zhang, W. J.; Leng, Y. K.; Xiong, Y. H. *Talanta* **2018**, *186*, 29−35.
(21) Farka, Z.; Jurik, T.; Kovar, D.; Trnkova, L.; Skladal, P. *Chem. Rev.* **2017**, *117*, 9973−10042.
(22) Park, K. S.; Kim, H.; Kim, S.; Lee, K.; Park, S.; Song, J.; Min, C.; Khanam, F.; Rashu, R.; Bhuiyan, T. R.; Ryan, E. T.; Qadri, F.; Weissleder, R.; Cheon, J.; Charles, R. C.; Lee, H. *ACS Nano* **2017**, *11*, 11425−11432.
(23) Chen, Y. P.; Xianyu, Y. L.; Wang, Y.; Zhang, X. Q.; Cha, R. T.; Sun, J. S.; Jiang, X. Y. *ACS Nano* **2015**, *9*, 3184−3191.
(24) Xianyu, Y. L.; Wang, Q. L.; Chen, Y. P. *TrAC, Trends Anal. Chem.* **2018**, *106*, 213−224.
(25) Zhang, Z.; Li, T.; Sheng, Y.; Liu, L.; Wu, H. C. *Small* **2019**, *15*, 1804078.
(26) Liu, L.; Li, T.; Zhang, S.; Song, P.; Guo, B.; Zhao, Y.; Wu, H. C. *Angew. Chem., Int. Ed.* **2018**, *57*, 11882−11887.
(27) Tong, S.; Ren, B. B.; Zheng, Z. L.; Shen, H.; Bao, G. *ACS Nano* **2013**, *7*, 5142−5150.
(28) Yuan, C.; Deng, Y.; Li, X.; Li, C.; Xiao, Z.; Liu, Z. *Anal. Chem.* **2018**, *90*, 8178−8187.
(29) Zhao, Y.; Yang, Y.; Sun, Y.; Cui, L.; Zheng, F.; Zhang, J.; Song, Q.; Xu, C. *Biosens. Bioelectron.* **2018**, *99*, 193−200.
(30) Xu, L. G.; Sun, M. Z.; Ma, W.; Kuang, H.; Xu, C. L. *Mater. Today* **2016**, *19*, 595−606.
(31) Toor, A.; So, H.; Pisano, A. P. *Appl. Surf. Sci.* **2017**, *414*, 373−379.
(32) He, L.; Musick, M. D.; Nicewarner, S. R.; Salinas, F. G.; Benkovic, S. J.; Natan, M. J.; Keating, C. D. *J. Am. Chem. Soc.* **2000**, *122*, 9071−9077.
(33) Kesama, M. R.; Yun, B. K.; Ha, T.; Dugasani, S. R.; Son, J.; Kim, J. H.; Jung, J. H.; Park, S. H. *Nanotechnology* **2018**, *29*, 465703.
(34) Chen, Y. P.; Sun, J. S.; Xianyu, Y. L.; Yin, B. F.; Niu, Y. J.; Wang, S. B.; Cao, F. J.; Zhang, X. Q.; Wang, Y.; Jiang, X. Y. *Nanoscale* **2016**, *8*, 15205−15212.
(35) Wang, Z. H.; Jin, G. *J. Immunol. Methods* **2004**, *285*, 237−243.
(36) Huang, C.; Yang, Q.; Song, F.; Chen, N.; Liao, X.; Yao, B.; Zhang, S.; Chen, Y.; Jin, G. *Integr. Ferroelectr.* **2016**, *171*, 70−78.
(37) Markel, V. A. *J. Opt. Soc. Am. A* **2016**, *171*, 1244−1256.
(38) Chen, Y. P.; Xianyu, Y. L.; Dong, M. L.; Zhang, J. J.; Zheng, W. S.; Qian, Z. Y.; Jiang, X. Y. *Anal. Chem.* **2018**, *90*, 6906−6912.
(39) Yan, C.; Zhang, J.; Yao, L.; Xue, F.; Lu, J.; Li, B.; Chen, W. *Food Chem.* **2018**, *260*, 208−212.

DOI: 10.1021/acs.analchem.9b00846
Anal. Chem. 2019, 91, 6769−6774